Netherlands Journal of Sea Research
25 (1/2): 31-44 (1990)

SUB-TIDAL DYNAMICS OF A NEAR-COASTAL ZONE IN THE NORTH SEA

J.J.M. VAN HAREN
Netherlands Institute for Sea Research, P.O. Box 59, 1790 AB Den Burg, Texel, The Netherlands

ABSTRACT

Data, gathered in the North Sea some 60 km north of the Netherlands, are used to describe the regional dynamics at sub-tidal frequencies. Using a tidally averaged set of the vertically averaged horizontal momentum equations, the influence of the separate terms in these equations is investigated experimentally. The results reveal that, especially further offshore, the wind driven motion is in (near) geostrophic balance. This confirms the ability to monitor the circulation, using information on the wind field and the bottom pressure distribution, within an accuracy equivalent to an accuracy of 0.5 mb of low pass filtered bottom pressure gauge measurements.

In a part of the area where the bottom topography reaches a slope of 1.2×10^{-3} and where density fronts are observed, the motion is frequently found out of geostrophic balance. The apparent imbalance can partly be attributed to 'sub-grid' horizontal density gradients, which are incorporated in the measured bottom pressure gradients, assuming that no sea-level adjustment occurs.

1. INTRODUCTION

A first analysis is presented of measurements of physical parameters obtained in June 1986 and July 1987 in an area of the North Sea of which the centre is 60 km north of the Netherlands at the transition of the Southern Bight and the Central North Sea. The area of interest, marked by the rectangle in Fig. 1, exhibits a diversity of transitions or gradients, which are larger than in the surrounding water and which generally show a large temporal and spatial variability. Transitions in biological and geological properties, which are rather persistent in time, are reported by CREUTZBERG (1985). Climatological atlasses show three different types of water masses, discriminating between Coastal, Channel and Central North Sea waters (LEE, 1980). The tidal currents decrease in amplitude towards the north, while the major axis is aligned with the isobaths (SAGER & SAMMLER, 1968). On seasonal time scales the thermal stratification parameter indicates a transition zone or tidal mixing front (PINGREE & GRIFFITHS, 1978). As far as the accuracy of the spatial distribution of the transition zones allows, the gradients seem to concentrate between the 30 and 40 m isobath, with the largest magnitudes in the cross-isobath direction. Whereas for the whole area the bottom topography is rather flat with a general slope of 0.4×10^{-3}, the slope between 30 and 40 m depth locally reaches 1.2×10^{-3}. In this paper physical processes are described which have time scales varying from two days to a month: sub-tidal processes.

From the, scarce, field experiments (THOMPSON & PUGH, 1986; HUTHNANCE, 1983; BROWN *et al.*, 1985) and models (WEENINK, 1958; ALLEN, 1980) describing motions on sub-tidal time scales in similar, shallow water, near coastal sea areas, it is known that wind driven motion is predominant as long as no density gradients or strongly varying topography are present. Regarding the position of the measurement area, near the central axis of the basin and in the vicinity of the southern coast, and regarding the time scales of the wind variations, typically two days, the wind driven motion will predominantly be directed along the coast and is expected to be found in a geostrophically balanced quasi-stationary state. For example, dominating, steady, westerly winds cause water to pile-up near the coast due to cross-isobath Ekman transport. The resulting cross-isobath pressure gradient will be balanced geostrophically, thus providing an along-isobath current. The current velocity perpendicular to the coast may show a considerable vertical shear, but the net horizontal transport has to be zero near the coast (WEENINK, 1958; GILL, 1982).

For an area with spatial and temporal density variations, additional motions and influences on the depth independent geostrophic motion are expected. The vertical, directly wind driven, current structure may substantially differ in stratified and in well mixed waters due to the limiting effects on vertical momentum transport by the stratification (CSANADY, 1982; MAAS & VAN HAREN, 1987). A horizontal density gradient or 'front' induces a motion which is geostrophically balanced and which may show a considerable vertical structure depending on the

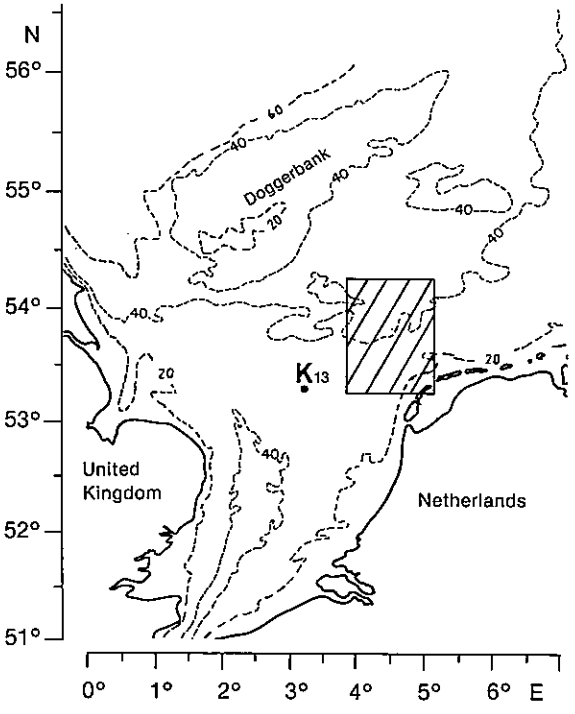

Fig. 1. Southern part of the North Sea, with the investigation area marked by the rectangle. Wind data were measured at platform K_{13}.

type of front (VAN AKEN *et al.*, 1987). If the position or strength of a front shows temporal variability, temporal variations in the density driven motion are expected (VAN HAREN & MAAS, 1987; VAN AKEN *et al.*, 1987).

In this paper the analysis of the different types of motion is focussed on the wind driven motion. As a result of this analysis the ability of bottom pressure gauges to describe a geostrophic motion with sufficient accuracy is tested. THOMPSON & PUGH (1986) have shown that in the Celtic Sea bottom pressure gauges register the sub-tidal pressure fluctuations with an accuracy better than 50 Pa (0.5 mb).

Acknowledgements.—I like to thank the crew of the R.V. 'Aurelia' for the pleasant cooperation during the cruises and C. Veth for his help in the organizing work. The CTD-data collected on board the R.V. 'Holland' were supplied by the North Sea division of the Dutch Ministry of Transport and Public Works. The bottom pressure gauge time series were supplied by the Hydrographic Service of the Royal Netherlands Navy, and I would like to thank H. Versteegh for the discussions on the interpretation of these data. I like to thank L. Maas for his numerous suggestions on the analysis of data in general. The author is supported by a grant of the Netherlands Organization for the Advancement of Scientific Research (NWO).

TABLE 1

Periods (in year-days) of available data in 1986 (a) and 1987 (b). The name of the current meters, *e.g.* 'A02.5,30', contains the distance from the bottom (02.5) and the local waterdepth (30) in m. Additional current meter sensors are indicated with T (thermistor) and S (conductivity cell).

name	*1986 period (days)*	*name*	*1987 period (days)*
currents:			
A05.5,31 T	149-181	A02.5,31 T	182-218
A11.0,31 T	149-165	A12.5,31 T	182-251
A16.5,31 T	149-181	A16.5,31 T	182-239
		A20.5,31 TS	182-251
B08.5,38 T	129-181	B02.5,38 TS	182-218
B14.0,38 T	129-181	B10.0,38 T	182-251
B19.5,38 T	129-181	B17.5,38 T	182-241
B25.0,38 T	129-181	B21.5,38 T	182-251
		B25.5,38 TS	182-232
C03.0,41 T	129-181	C02.5,41 TS	188-218
C09.5,41 T	129-181	C12.5,41 T	182-251
C16.0,41 T	129-181	C22.5,41 T	182-251
C22.5,41 T	129-181	C26.5,41 T	182-251
C29.5,41 T	129-181		
D13.0,27	147-182	D02.5,29 T	182-251
		D09.0,29	182-222
		D14.5,29 T	182-231
E05.0,38	147-182	E02.5,38 T	182-245
E23.0,38	147-182	E17.0,38	182-245
		E24.5,38 T	182-245
F06.0,44	147-182	F02.5,44 T	196-226
F31.0,44	147-182	F24.0,44	182-196
		F31.5,44 T	182-245
G06.0,48	147-182	G25.0,48	182-245
G35.0,48	147-182		
		I02.5,37 T	207-245
		I15.0,37	182-238
		I25.5,37 T	182-245
pressure:			
A	147-182	A	182-224, 225-257
B	147-182	B	182-224, 225-257
		C	225-257
D	147-182	D	182-224, 225-257
E	147-182	E	182-224, 225-257
F	147-182	F	182-224, 225-257
G	147-182	G	182-224, 225-257
I	147-182	I	182-224, 225-257
CTD:			
AURELIA	128-130,134-135, 146-150,154-155, 160-163,167-170, 181-184	AURELIA	179-182, 215-216, 222-225,230-233, 236-237,243-246
HOLLAND	146-149,160-163, 167-170	HOLLAND	209-213,222-225, 230-232

2. DATA

Fig. 2a shows the positions of the moorings containing current meters and bottom pressure gauges. The available amount of data from both periods in 1986 and 1987 is given in Table 1. Fig. 2b shows the bathymetry along the y-axis with the steepest slope of 1.2×10^{-3} between A and B. During both measurement campaigns the same mooring positions were used. All current meters marked with T in Table 1 were equipped with thermistors. In 1987 four current meters, marked with S in Table 1, additionally returned conductivity data, which were only reliable for the first three weeks of measurements due to contamination of the sensors. From two ships CTD measurements were performed in different parts of the area during different periods. The distance between the CTD stations varied from 3-14 km. Wind data measured at platform K_{13} were available at intervals of 6 hours. From the available data the periods June 1986, year-days 149-181, and July 1987, year-days 183-217, were selected for the obvious reason that in these periods the maximum number of records could be used. The vector time series of wind stress ($\vec{\tau}$) and currents ($\vec{u}$) are divided into two separate time series, $\vec{\tau} = (\tau_x, \tau_y)$ and $\vec{u} = (u, v)$ respectively, along the horizontal coordinates (x,y) as defined in Fig. 2a. The x-coordinate is aligned on average with the 30 m isobath. The pressure gauge series p' are defined as the fluctuations around their mean value, which is obtained by averaging over the total span of time. To remove the tides all time series have been filtered using a generalized type of low pass Hanning filter as described by CARTWRIGHT (1983). The proper filter used by Cartwright has been slightly modified in its properties because of the undesirable large number of end points lost. In Table 2 and Fig. 3 a comparison of the proper and the modified filter is made in terms of the filter properties and their amplitude response functions. Although some 5% of the energy at the O_1-frequency passed

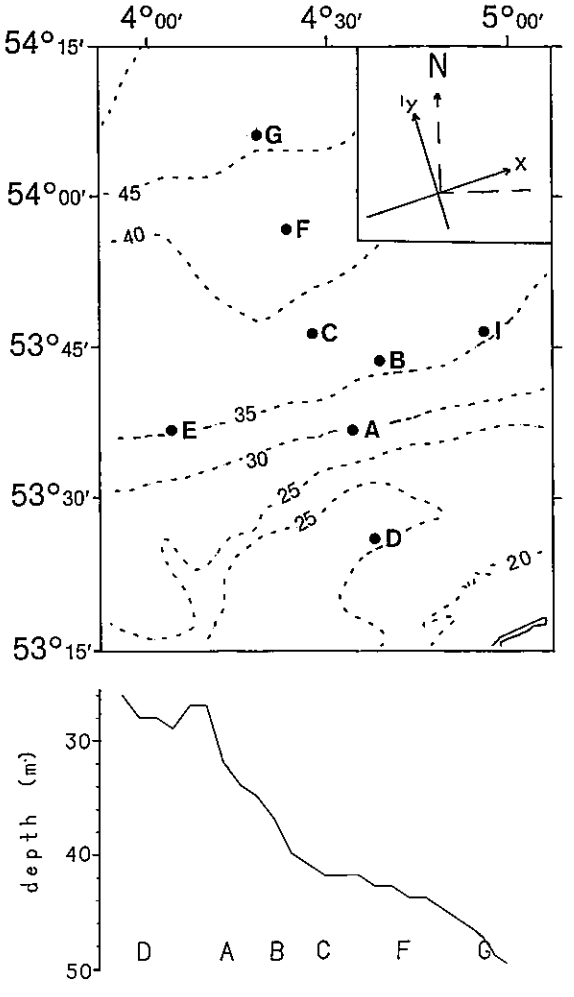

Fig. 2. (a) Mooring positions indicated with the letters A-I. Isobaths are drawn every 5 m. In the upper right the coordinate system used is sketched. The origin is located at the intersection of the lines D-G and E-I. (b) Bottom topography along the y-axis.

TABLE 2

Properties of the low pass filters used on our data (I) and used by CARTWRIGHT (1983) (II).

		I	II
number of end points lost	(days)	2 x 3	2 x 7
half amplitude cut off frequency	(cpd)	0.75	0.75
highest total pass frequency	(cpd)	0.5	0.64
'first zero' frequency	(cpd)	1.0	0.86

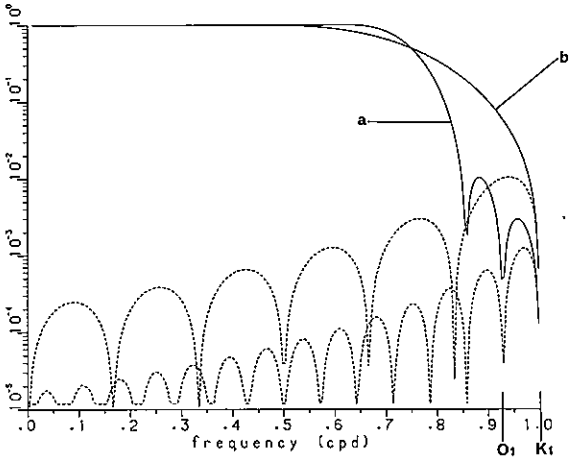

Fig. 3. Amplitude response functions (solid lines) for the proper (a) and modified (b) filters together with the (back-folded) first aliased portions (dashed) as a function of frequency. Indicated are some tidal frequencies.

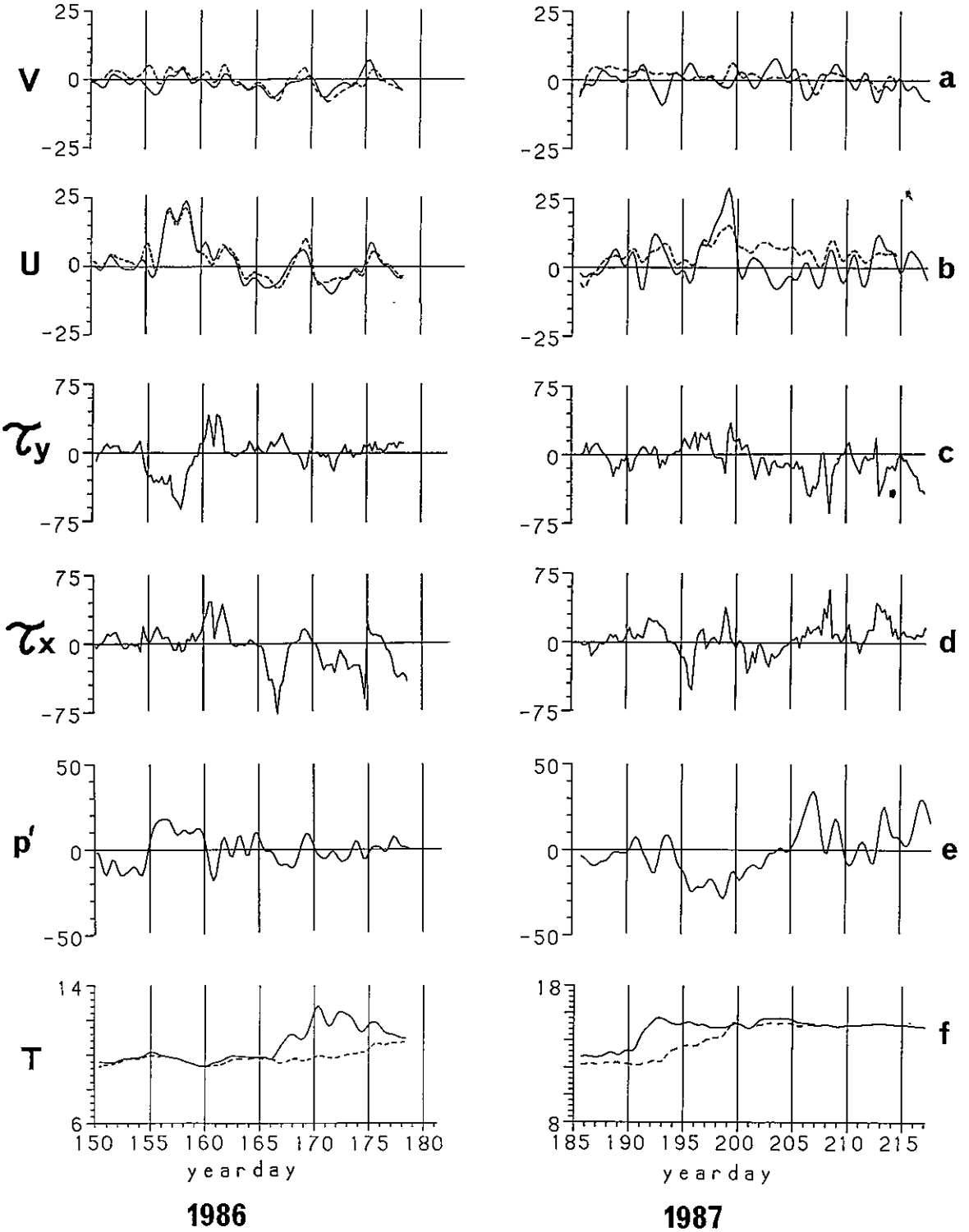

Fig. 4. Low pass filtered time series for mooring B and wind station K_{13} : (a) cross-isobath current (cm/s); (b) along-isobath current (cm/s); (c) cross-isobath wind stress (x0.01 N/m^2); (d) along-isobath wind stress (x0.01 N/m^2); (e) pressure fluctuations (mb); (f) temperature (°C). In (a), (b) and (f) the solid line represents the uppermost current meter record and the dashed line the lowest.

the modified filter, the results by use of either filter agree well and are better than from a similarly tested twice operated 25 hours running mean filter.

3. OBSERVED SUB-TIDAL TIME SERIES AND HYDROGRAPHY

Filtered series, measured at mooring B and wind station K_{13}, are depicted in Fig. 4 as a function of time for June 1986 and July 1987. The time is given in year-days. The wind stress components are plotted according to the oceanographic convention. For both periods the currents in the along-isobath direction show larger amplitudes than in the cross-isobath direction. The vertical current-shear has magnitudes of $O(10^{-3}\text{-}10^{-2}\ s^{-1})$ for both directions. In the horizontal plane the currents show some shear, with the maximum along-isobath currents generally found at A. In order to determine a measure for the relationship between time series, squared coherencies have been calculated, which have been compared with the significant value at the 95%-confidence level. From the calculations three mutually unrelated frequency bands are selected, which are centered around 0.1, 0.31 and 0.51 cpd. Although not all series of a 'type' (*e.g.* 'u-current') show the same results and despite some differences between the two periods, the results shown in Table 3 may be regarded as typically for the lowest and the highest frequency bands. From Table 3 and Fig. 4, the cross-isobath wind stress is found in coherence with the pressure fluctuations, especially in the 0.1 cpd frequency band. This indicates that a stronger onshore wind leads to a rise of the (overall) sea level. To a lesser extent along-isobath winds are coherent with the along-isobath currents. Tests for the 1986 time-series from day 160 onward showed coherence between the along-isobath wind stress and the along-isobath currents (not shown in Table 3). High coherence has been found between the pressure gradient in the y-direction and the along-isobath currents, especially in the 0.51 cpd frequency-band. This supports the notion of wind driven along-isobath currents that are found in a geostrophically adjusted state (GILL, 1982). Somewhat puzzling is the coherence found between the bottom temperature gradient in the y-direction and the along-isobath currents for the low-frequency band in 1987. The non-coherence observed between the pressure gradient and the along-isobath currents in the same period for the same band will be described in the consecutive sections.

Typical temporal fluctuations of temperature are depicted in Fig. 4f. In 1986 a gradual temperature increase was observed, with a sharp increase in the upper layers between days 167-170. Before day 165 the water was vertically well mixed for nearly the whole area, with the (slightly stratified) colder and less saline water in the north. Till this day a surface to bottom haline front existed between stations A and B. A bottom thermal front was gradually generated northward from the haline front. After development both fronts combined in a surface density front. After day 165 strong thermal stratification was observed firstly in the north, whereas in this period the less saline water was found in the south. The apparent reversal of the horizontal salinity gradient is illustrated by the density distributions at 20 m depth for days 163 and 182 (Fig. 5a, c). Probably the easterly winds prevailing from day 165 onwards replaced the high salinity Channel water in the south by less saline Coastal water. Maximum horizontal density gradients, reaching up to 0.15 kg/m^3/km, have been observed between A and B near the position of the steepest slope (Fig. 5b).

For technical reasons the positions of the uppermost current meters were 10-15 m below the surface. Compared with the shallow depth of the thermocline this positioning limits a thorough description of the

TABLE 3

Typical phase differences in degrees between time series related coherently with 95%-confidence. The column leads the row in phase; when no phase is shown the coherency has been found below the confidence level. (a) 0.1 cpd frequency band; (b) 0.51 cpd frequency band

	v	τ_x	τ_y	p'	$\partial p'/\partial y$	$\partial T_b/\partial y$
u	0^+				180*	180**
	v	20^+			180*	180**
		τ_x				
			τ_y	190		
				p'		
					$\partial p'/\partial y$	

$^+$ = 1986 only;
* = 1986 only; not for stations D, A;
** = 1987 only; not for station D

(a)

	v	τ_x	τ_y	p'	$\partial p'/\partial y$	$\partial T_b/\partial y$
u	350^x	330	180	90^x	190	
	v	350^+			220^x	
		τ_x				
			τ_y	240	350^x	
				p'	100^x	
					$\partial p'/\partial y$	

$^+$ = 1986 only;
^{x} = 1987 only;

(b)

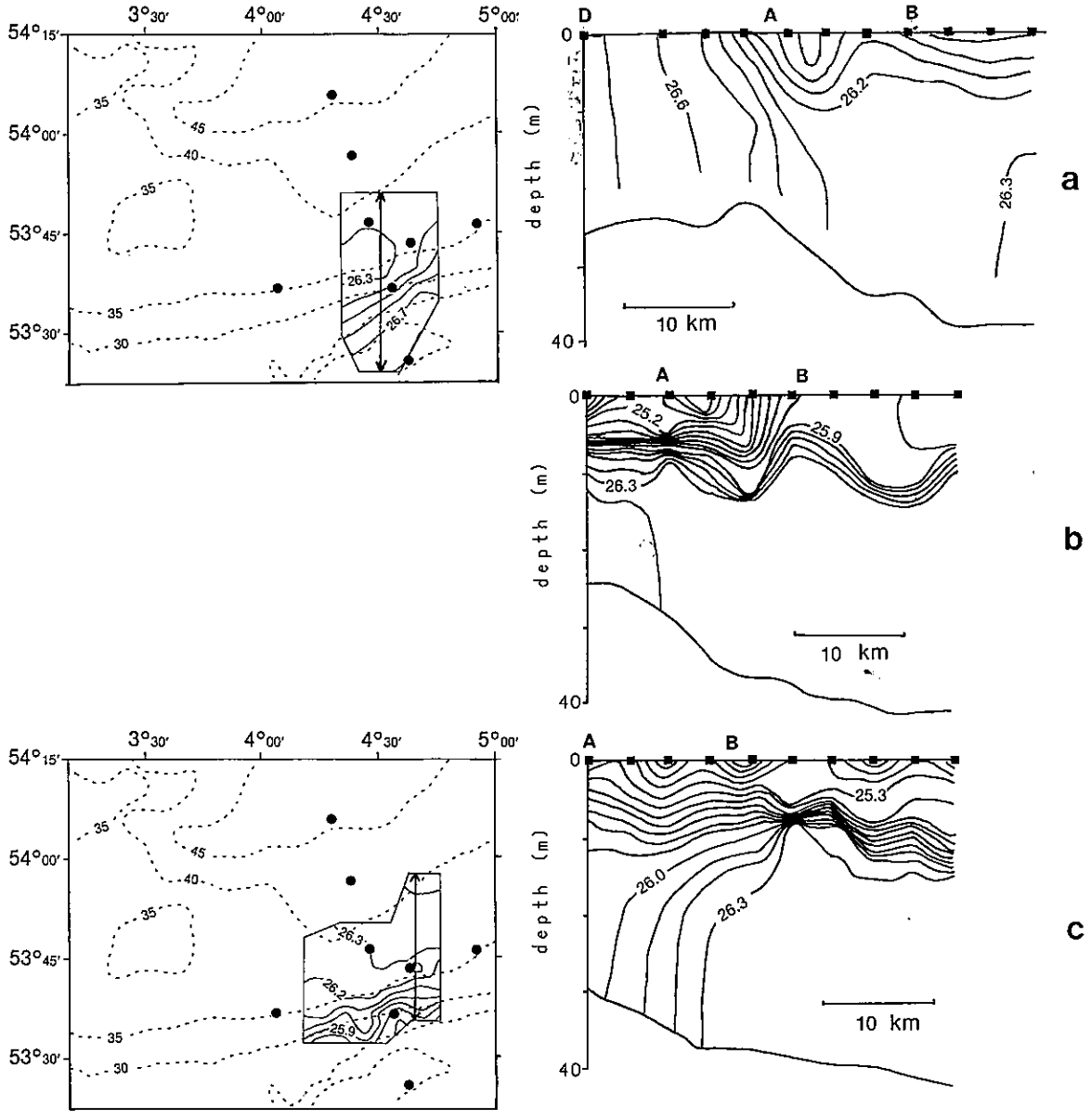

Fig. 5. Horizontal (at 20 m depth) and vertical sections of density excess (γ in kg/m^3) for the periods: (a) day 163, 1986 (b) day 168,1986, vertical section along 4°30'E; (c) day 182, 1986; (d) day 183, 1987; (e) day 210, 1987. CTD-stations are represented by (■); current meter moorings by (●); the positions of the vertical sections are indicated in the horizontal sections (by an arrow).

temperature distribution from observations in 1987. Unfortunately no CTD-data are available between days 183 and 210. As far as possible to observe from the time series, July 1987 shows thermal stratification between days 190-195 for A, between 190-200 for B and between 190-207 for all northerly stations. After day 207 all remnant stratification has been destroyed during a period with strong winds (Fig. 4f, 4c). From the CTD-observations at days 183 and 210 a frontal zone, mainly determined by salinity, is found east of the mooring axis y (Fig. 5d, 5e). This boundary between Coastal and Central North Sea waters shows the largest gradients near the surface, but extends towards the bottom. The low salinity water has hardly been observed at the stations A and B, except between days 184-196 when the practical salinity (S)

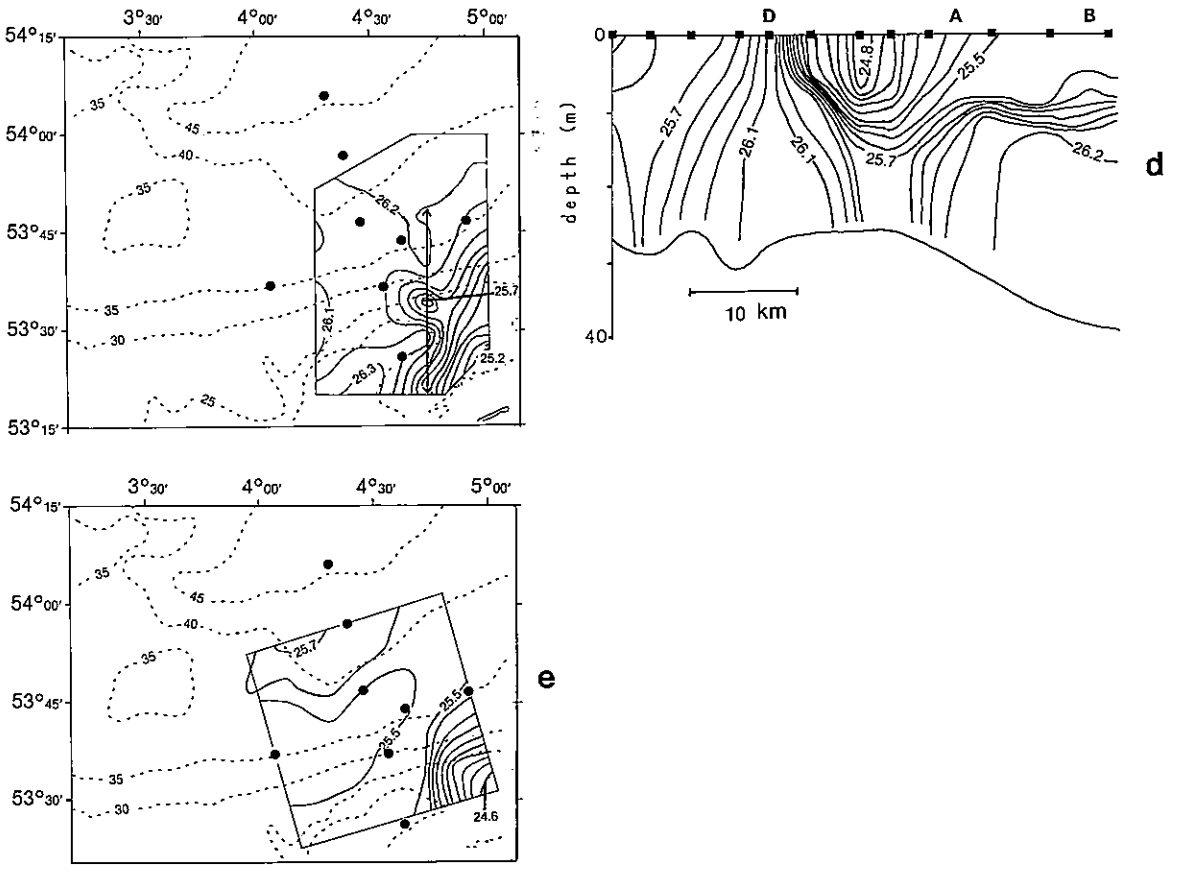

Fig. 5 continued.

observed at the upper current meters was 0.1-0.2 lower at station A than at station B, in contrast with the observation in the rest of the period. After day 207 a general decrease in salinity has been observed at A, B and C, accompanied by strong contamination of the near-bottom conductivity sensors. The relation between the general decrease in salinity and the larger decrease in the salinity time series of the bottom current meters, attributed to contamination of the sensors, has not been investigated.

4. EQUATIONS FOR SUB-TIDAL MOTION

In order to investigate the contributions of the forces per unit mass in the equations governing the wind driven motion, the vertically and tidally averaged horizontal momentum equations read, in the (x,y) coordinate system:

$$\frac{\partial \langle u \rangle}{\partial t} + \langle u \frac{\partial u}{\partial x} \rangle + \langle v \frac{\partial u}{\partial y} \rangle - f \langle v \rangle = - \langle \frac{\partial p'}{\varrho \partial x} \rangle + \langle \frac{s\tau_x}{\varrho(H+\zeta)} \rangle - \langle \frac{\alpha C_d |\vec{u}| u}{H+\zeta} \rangle \qquad (1a)$$

$$\frac{\partial \langle v \rangle}{\partial t} + \langle u \frac{\partial v}{\partial x} \rangle + \langle u \frac{\partial v}{\partial y} \rangle + f \langle u \rangle = - \langle \frac{\partial p'}{\varrho \partial y} \rangle + \langle \frac{s\tau_y}{\varrho(H+\zeta)} \rangle - \langle \frac{\alpha C_d |\vec{u}| v}{H+\zeta} \rangle \qquad (1b)$$

(a) (b) (c) (d) (e) (f)

where the tidal averaging operator is denoted by $< >$, and with:

$$u = \frac{1}{H+\zeta} \int_{-H}^{\zeta} u\, dz, \quad v \text{ similar; vertically averaged velocity}$$

H	waterdepth
ζ	sea level fluctuations
f	$=1.175\times10^{-4}$ s^{-1} inertial frequency (53°40'N)
p'	bottom pressure fluctuations
ϱ	density of sea water
τ_x, τ_y	wind stress in x,y-direction
s	=1.07; explained below
α	$=0.55^2$; explained below
C_d	$=2.5\times10^{-3}$ drag coefficient for bottom friction

In the horizontal momentum equations lateral friction has been assumed to be much smaller than bottom friction and wind forcing. To obtain eq. (1) the general horizontal momentum equations have been vertically averaged first, in which the advection terms have been approximated according to:

$$\overline{u\partial u/\partial x + v\partial u/\partial y} \approx u\partial u/\partial x + v\partial u/\partial y,$$

and similarly for the y-direction (HEAPS, 1978). Due to the uncertainty of the overall datum or geopotential in each series p', the overall time mean of each term in eq. (1) has been removed.

In order to obtain information on the spatial distribution of the force terms, calculations of these terms are performed by means of all pairs of moorings that lie on a line that coincides more or less with one of the adopted coordinate axes. Due to the geometry of the set of mooring positions only for one (central) position the total advection terms (b) can be calculated. However, these terms are small, as will be shown.

In the bottom friction term (f) a constant drag coefficient is used. To relate the bottom current velocity to the depth averaged velocity the latter is multiplied with a factor of $\sqrt{\alpha}$=0.55. Both values are adopted from MAAS & VAN HAREN (1987). WEENINK (1958) has calculated a value of s=1.07 with which the wind stress in term (e) has to be multiplied. The resulting 'effective' wind stress has been introduced in order to allow for bottom stress in the case that the vertically averaged velocity vanishes. The wind stress has been calculated in the usual way, using a drag coefficient which depends on the wind velocity (BOWDEN, 1983).

Table 4 and Fig. 6 show the standard deviations and sub-tidal fluctuations, respectively, of all terms in eq. (1) calculated by means of measurements at the moorings F and G (denoted FG) for the y-direction and E and B (denoted EB) for the x-direction in 1987. The standard deviations of the advection terms (b) have been calculated for position B. Calculations by means of other mooring pairs will be considered in section 5. Clearly only three terms are important: (c), (d) and (e), with (c) and (d) dominating (e) for the y-direction. Thus, in general a geostrophic balance is found and the assumption of a quasi-steady state is valid.

TABLE 4

Typical standard deviations of force terms per unit mass calculated according to eq. (1) by means of data from the mooring pairs FG (y-axis) and EB (x-axis) in 1987. Standard deviations of the advection terms (b) have been calculated for mooring B and are indicated between brackets.Included are the standard deviations for the 'error' series, defined as the residual series after summing all force terms of eq. (1), and the errors in individual pressure records as derived from the error series' standard deviation following THOMPSON & PUGH (1986).

force term of eq. (1)	*standard deviations (in 10^{-5} m/s^2)*	
	FG (y-axis)	*EB (x-axis)*
(a)	0.06	0.09
(b) (mooring B)	(0.02)	(0.02)
(c)	0.65	0.20
(d)	0.61	0.23
(e)	0.26	0.35
(f)	0.01	0.06
error series	0.34	0.30
	errors (in mb)	
pressure series	0.44	0.86

THOMPSON & PUGH (1986) have calculated an upper-bound error in the sub-tidal bottom pressure fluctuations from the standard deviation of the 'error series', resulting after summing up all terms in each of the eq. (1). Assuming the error in the pressure gradient to be equally due to the errors in the respective series p', they have found an error in p' smaller than 0.5 mb, which is also found for FG in Table 4. However, this error in p' seems to be too large if it is compared with the error calculated from the error in the individual measurements. Taking an individual measurement error of 2.5 mb (Versteegh, pers. comm.) and assuming low pass filtering to be equal to averaging over 100 data-points (24 hours), an error in p' of 0.25 mb is found. Other error sources, which may contribute to the standard deviation of the error series, are the determination of the vertical average of the currents, fluctuations in density and contributions by the tidal stress on unresolved smaller horizontal length scales.

For a description of the deviations from a wind induced geostrophic balance we consider the

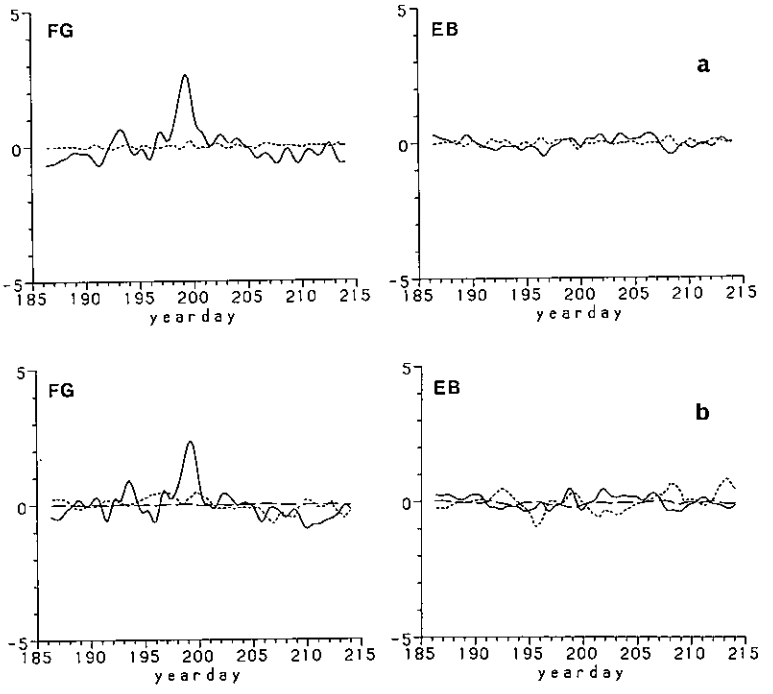

Fig. 6. Time series of forces per unit mass (in 10^{-5} m/s^2) calculated from eq.(1) between the moorings FG (y-direction) and EB (x-direction) in 1987. (a) Terms at the left hand side of eq. (1): (----)=(a), (———)=(c). (b) Terms at the right hand side of eq.(1): (———)=(d), (---)=(e), (— —)=(f).

hydrostatic equation relating the pressure to the sealevel and density. According to this relation a bottom pressure gauge measures a total pressure p(t):

$$p(t) = p_a(t) + \int_{-H(t)}^{\zeta(t)} g\varrho(z,t)\, dz$$

where $p_a(t)$ denotes the atmospheric pressure fluctuations, g=9.81 ms^{-2} the acceleration of gravity and $H(t)$ the waterdepth, which shows a time dependency to allow for interperiodical datum shifts due to instrument displacements. As the exact local height of the geopotential is unknown, only pressure fluctuations $p'(t)$ around a local (time) mean can be used for calculations:

$$p'(t)=p_a'(t)+g\bar{\varrho}\zeta'(t)+g\bar{\varrho}H'(t)+\int_{-<H>}^{0} g\varrho'(z,t)dz \qquad (2)$$

with $\bar{\ }$ denoting the time and depth mean, < > the time mean and ' the fluctuations around their respective means. After low pass filtering, the first two terms on the right hand side of (2) describe the atmospherically ('wind') induced pressure fluctuations, considering the unknown sea level fluctuations solely due to wind effects. The third term does not induce any motion at all. The gradient of the last term describes the density driven motion when horizontal gradients in the local density fluctuations occur. The last term in eq. (2) then may be regarded as a perturbation on the wind driven part of the pressure fluctuations, induced by density differences, assuming that no sea level compensation occurs. Note that this term depends on the total waterdepth, which may be a function of x,y as are ϱ, ϱ', ζ' and in a much weaker sense p_a'.

5. FORCE BALANCE OBSERVATIONS

From the results of calculations of the terms in eq. (1), only those obtained by means of consecutive pairs of moorings are presented in this chapter. An abbrevation like 'AB' denotes 'by means of moorings A and B' or a force balance valid for the stretch from mooring A to B. Firstly the balance between the Coriolis term (c) and the pressure gradient term (d) will be considered, followed by a comparison of the wind stress term (e) with deviations from a geostrophic balance. Although the balance between the force terms is reasonable for the x-direction, we restrict the

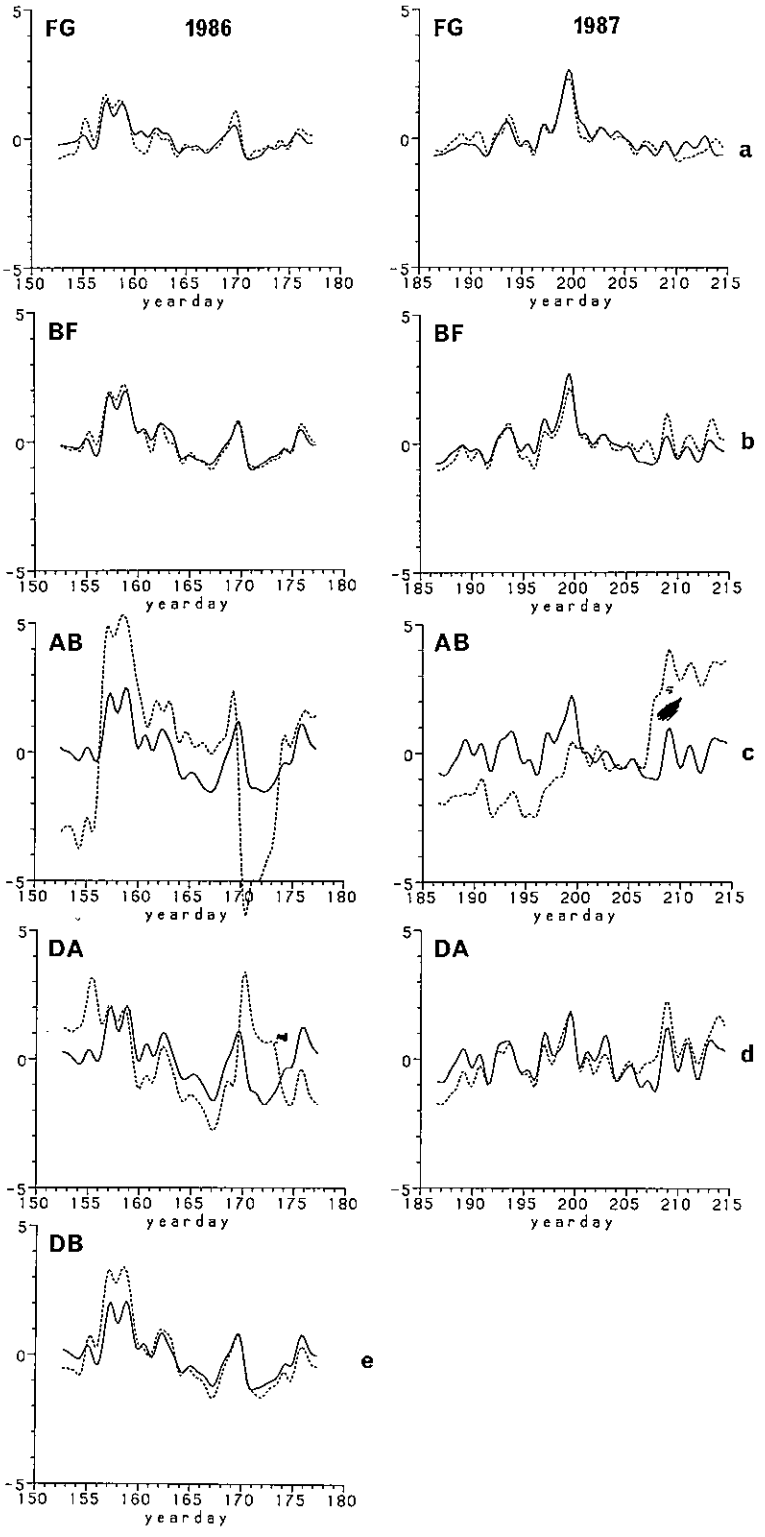

Fig. 7. Comparison of Coriolis force terms (c) (solid lines) and pressure gradient terms (d) (dashed lines) from eq. (1b) in 10^{-5} m/s^2 as a function of time for consecutive pairs of moorings (indicated by double letter-names).

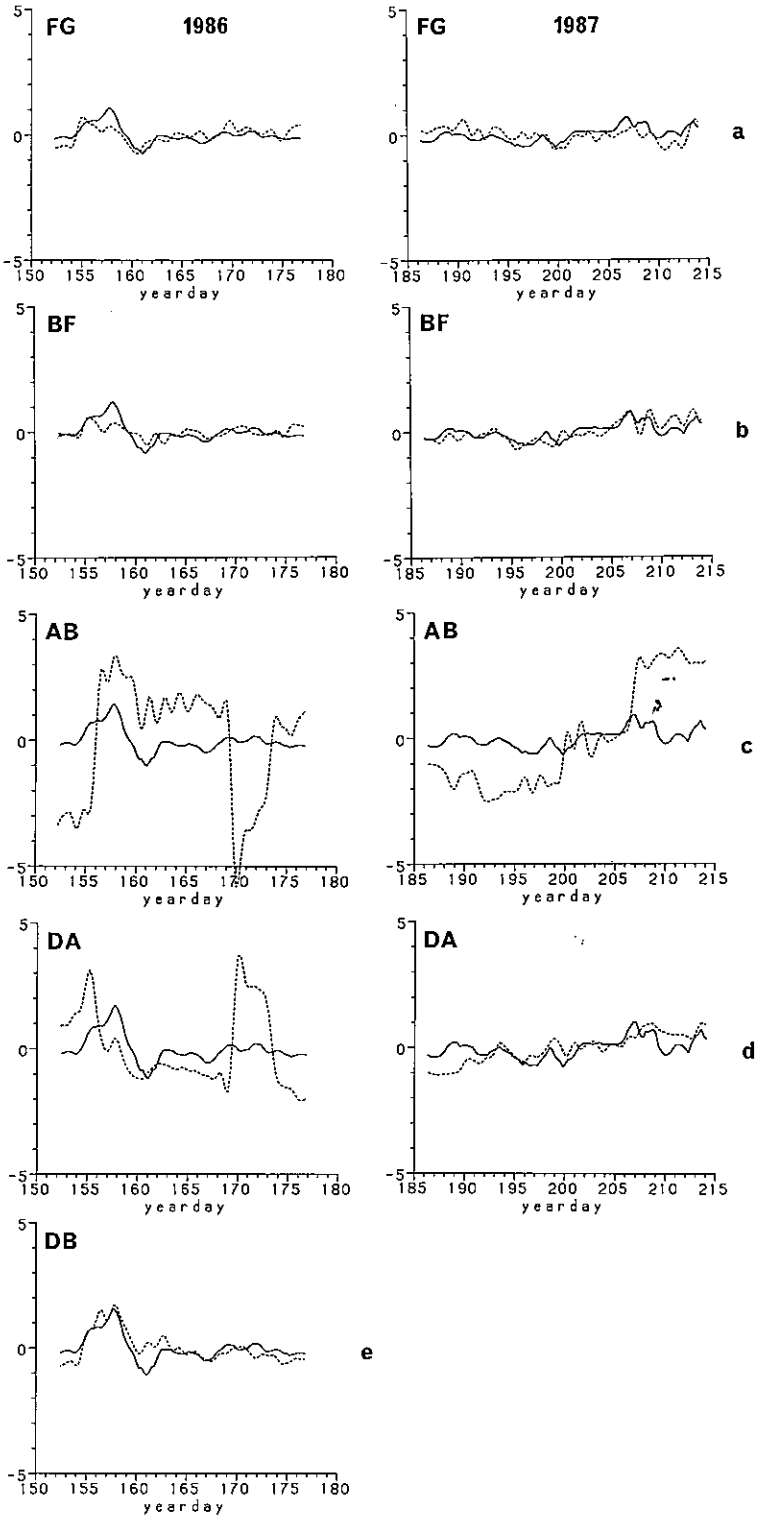

Fig. 8. Wind stress terms (e) (solid lines) from eq. (1b) and a-geostrophic portions (c)-(d) from Fig. 7 (dashed lines) in 10^{-5} m/s^2 as a function of time.

discussion to the balance between the more dominant terms for the cross-isobath (y) direction. Because of pressure gauge failure, mooring C has been excluded from the calculations, curiously enough in both periods. The parameters and assumptions as described in section 4 remain unchanged for all calculations.

The degree of geostrophic balance, calculated between each pair of consecutive moorings, is shown in Fig. 7. For reasons to be explained the balance for DB is included in Fig. 7e. From the Figs 7a and 7b for each period a (near)geostrophic balance is found between the moorings northward of B. The agreement between the two force terms is good, both in gross form and on a small time scale. The southerly stations give less balanced results (Fig. 7c, d), not so much in the fluctuations on smaller time scales but because of sudden step-like 'datum-shifts' of the pressure gradient term. The observed imbalance in 1987 is most pronounced for AB (Fig. 7c), with the pressure gradient term less than the Coriolis term till day 200, in balance between days 200-207 and too large after day 207. Although BF and DA (Fig. 7b,d) show a similar trend, their observed imbalance is much smaller, which supports the idea that an instrumental error is rather unlikely. Actually, it is unlikely that two or more instruments (D and A or B, F and G) at the same time show a datum shift due to instrument displacement. A physical explanation is suggested in section 6.

Station A, 1986, definitely showed an instrument caused datum shift of 40 mb within 45 minutes at day 169, curiously enough about 18 hours after a similar shift occurred at station I. After removal of these shifts a large imbalance remained for AB and DA (Fig. 7c, d). Regarding the degree of geostrophic balance until day 169, a large imbalance shift occurs for AB at day 156. DA seems to be in geostrophic balance between days 155-160, whereas for DB (Fig. 7e) a geostrophic balance is found except for the period between days 155-160.

Fig. 8 shows the a-geostrophic portions of the momentum balances of Fig. 7, plotted as a function of time together with the wind stress terms. July 1987 was marked by moderate winds, which is reflected in Fig. 8 by the small contribution of the wind stress term. In this period, the magnitude of the a-geostrophic portions is small too. The wind stress explains the observed imbalance to a reasonable extent, except for AB.

In June 1986 a period of strong onshore winds occurred between days 155-160 (Figs 4c and 8). Again, the wind stress term accounts to a reasonable degree for the a-geostrophic portions, especially for FG, BF and DB. Some misfits remain, with an overestimate of the wind stress influence compared

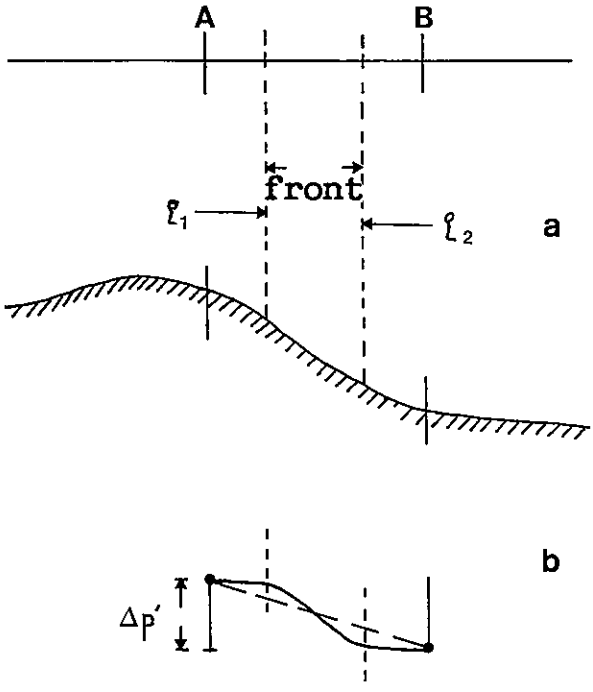

Fig. 9. (a) Model of a frontal zone between moorings A and B. (b) The associated density induced relative pressure (solid line) compared with the uniform pressure trend (dashed line) used for the calculations of term (d) in eq. (1).

to the a-geostrophic portions for BF and FG between days 157-160 and an underestimate for AB. In contrast with the observations in 1987 both DA and AB show large imbalances. Over the total stretch (*i.e.* for DB) the wind stress term explains the observed imbalance.

6. DISCUSSION

Before discussing the results obtained it is worthwhile to point out the 'lacking' data. Firstly, the vertical positioning of current meters has been rather unfortunate in relation to the depth of the pycnocline. As the pycnocline generally has been above the uppermost current meter, an unresolvable mix-up of depth dependent and independent motions is expected in the time series. Secondly, the general horizontal spacing of the CTD-stations (7 km) has been too wide in frontal zones. Thirdly, the number of conductivity time series has been too small for a thorough determination of the time evolution of the density distribution. CTD observations showed a more or less equal contribution of salinity and temperature to the density.

Despite large error premisses for working with pressure gauges (*e.g.* Versteegh pers. comm.) the results given in section 4 suggest that monitoring the

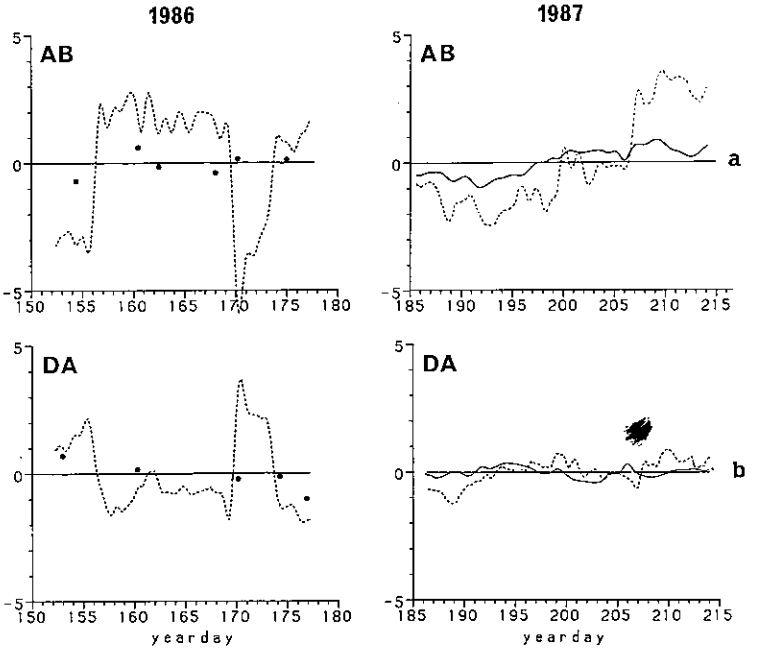

Fig. 10. Comparison between time series of the errors in eq. (1) (dashed lines) and the density induced pressure gradient forces per unit mass (solid lines and dots) in 10^{-5} m/s^2 for the mooring pairs DA and AB. The latter time series are obtained from pressure time series calculated according to the last term in eq. (2), for which the densities are taken from CTD-measurements in 1986 and from records provided by the additional current meter sensors in 1987.

wind driven circulation is possible with measurements of the wind field at a single station together with, at least three, bottom pressure gauges which provide time series with an accuracy of 0.5 mb or better. This upper boundary for the errors, calculated from the deviations of a balance in the momentum equations, presumably includes errors due to the determination of the true vertically averaged current from a small number of current meters and errors due to (small) density gradients. The smallest errors are found for deeper waters further offshore, where a pycnocline most likely exists, but where the bottom topography is rather smooth and where horizontal density gradients are small.

The basic idea for a first possible candidate for the missing force term to explain the imbalance observed for AB is that density induced geostrophic flow is restricted to the position of fronts (VAN HEIJST, 1985), which generally have their largest gradients between A and B (Fig. 5). Therefore this motion is often not measured by the current meters at A or B but the frontal zone may still have its influence on the measured pressure fluctuations at these positions through the last term in eq. (2). A schematic view, in which the shape of the front is not important, is depicted in Fig. 9a. Due to the more localised, 'subgrid', density gradients a non-uniform pressure gradient is to be expected between A and B as sketched in Fig. 9b. From this figure the imbalance observed in section 5 is immediately explained as an overestimation of term (d) in eq. (1) due to the assumption of a uniform pressure gradient between the mooring stations.

The densities used in the calculation of the last term in eq. (2) have resulted from CTD-measurements in 1986 and from current meter records in 1987. Where no conductivity sensors have been in use in 1987, the density time series have been calculated from the temperature time series assuming a constant salinity, which value has been obtained from CTD-observations. From the time series of the last term in eq. (2) the temporal mean has been removed before the density induced pressure gradient force term has been obtained. Results are shown in Fig. 10, where the 'error' series, *i.e.* the residual time series of the force terms in eq. (1), are plotted as a function of time together with the density induced pressure gradient time series. The latter time series, called 'density' series, show a trend similar to the error series', but have a much smaller amplitude of about 0.3 of the error series. For AB roughly 20% of the density induced pressure gradient term has been due to the steep bottom slope. The validity of the calculated density series is difficult

to determine. The uncertainty in the individual density measurements is small (estimated to be smaller than 10% or 0.05 kg/m^3). However, it is unknown how large the uncertainties are due to the unresolved upper 10 m of the watercolumn and due to the poor vertical resolution of the salinity measurements (in 1987) or due to the little information on the time evolution of the density field (in 1986). Recall that the uncertainty in the error series amounts $\pm 0.3 \cdot 10^{-5}$ m/s^2.

7. REFERENCES

AKEN, H.M. VAN, G.J.F. VAN HEIJST & L.R.M. MAAS, 1987. Observations of fronts in the North Sea.—J. Mar. Res. **45:** 579-600.

ALLEN, J.S., 1980. Models of wind-driven currents on the continental shelf.—Ann. Rev. Fluid Mech. **12:** 389-433.

BOWDEN, K.F., 1983. Physical oceanography of coastal waters. Ellis Horwood Ltd., Chichester: 1-302.

BROWN, W.S., N.R. PETTIGREW & J.D. IRISH, 1985. The Nantucket Shoals Flux Experiment (NSFE79). Part II: the structure and variability of across-shelf pressure gradients.—J. Phys. Oceanogr. **15:** 749-771.

CARTWRIGHT, D.E., 1983. On the smoothing of climatological time series with application to sea-level at Newlyn.—Geophys. J. R. Astr. Soc. **75:** 639-658.

CREUTZBERG, F., 1985. A persistent chlorophyll *a* maximum coinciding with an enriched benthic zone. In: P.E. GIBBS. Proceedings of the nineteenth EMBS, Cambridge: 97-108.

CSANADY, G.T., 1982. Circulation in the coastal ocean. Reidel Publishing Company, Dordrecht: 1-279

GILL, A.E., 1982. Atmosphere-Ocean dynamics. Academic Press Inc., Orlando: 1-662.

HAREN, J.J.M. VAN & L.R.M. MAAS, 1987. Temperature and current fluctuations due to tidal advection of a front.—Neth. J. Sea Res. **21:** 79-94.

HEAPS, N.S., 1978. Linearized vertically-integrated equations for residual circulation in coastal seas.—Dt. hydrogr. Z. **31:** 147-169.

HEIJST, G.J.F. VAN, 1985. A geostrophic adjustment model of a tidal mixing front.—J. Phys. Oceanogr. **15:** 1182-1190.

HUTHNANCE, J.M., 1983. Sub-tidal motion on the Scottish continental shelf, August-September 1971.—Cont. Shelf Res. **1:** 221-236.

LEE, A.J., 1980. North Sea: physical oceanography. In: F.T. BANNER, M.B. COLLINS & K.S. MASSIE. The North-West European Shelf seas: the sea bed and the sea in motion. II. Physical and chemical oceanography, and physical resources. Elsevier Scientific Publishing Company, Amsterdam: 467-493.

MAAS, L.R.M. & J.J.M. VAN HAREN, 1987. Observations on the vertical structure of tidal and inertial currents in the central North Sea.—J. Mar. Res. **45:** 293-318.

PINGREE, R.D. & D.K. GRIFFITHS, 1978. Tidal fronts on the shelf seas around the British Isles.—J. Geophys. Res. **83**(C9)**:** 4615-4622.

SAGER, G. & R. SAMMLER, 1968. Atlas der Gezeitenströme für die Nordsee, den Kanal und die Irische See. Rostock.

THOMPSON, K.R. & D.T. PUGH, 1986. The subtidal behaviour of the Celtic Sea-II Currents.—Cont. Shelf Res. **5:** 321-346.

WEENINK, M.P.H., 1958. A theory and method of calculation of wind effects on sea levels in a partly-enclosed sea, with special application to the southern coast of the North Sea.—KNMI-mededelingen en verhandelingen no 73. Staatsdrukkerij en Uitgeverijbedrijf, Den Haag: 1-111.